

Nonlinear Optical Properties of Type I Collagen Fibers Studied by Polarization Dependent Second Harmonic Generation Microscopy

Adam E. Tuer,[†] Serguei Krouglov,[†] Nicole Prent,[†] Richard Cisek,[†] Daaf Sandkuijl,[†] Kazuhiro Yasufuku,[‡] Brian C. Wilson,[§] and Virginijus Barzda^{*†}

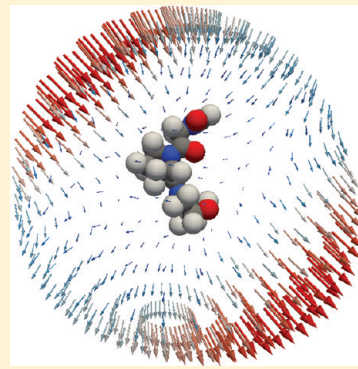
[†]Department of Physics, Institute for Optical Sciences, and Department of Chemical and Physical Sciences, University of Toronto, 3359 Mississauga Road North, Mississauga, Ontario, LSL 1C6, Canada

[‡]Division of Thoracic Surgery, Toronto General Hospital, University of Toronto, 200 Elizabeth Street, Toronto, Ontario, M5G 2C4, Canada

[§]Department of Medical Biophysics, University of Toronto, Ontario Cancer Institute, Princess Margaret Hospital, 610 University Avenue, Toronto, Ontario, M5G 2M9, Canada

 Web-Enhanced

ABSTRACT: Collagen (type I) fibers are readily visualized with second harmonic generation (SHG) microscopy though the molecular origin of the signal has not yet been elucidated. In this study, the molecular origin of SHG from type I collagen is investigated using the time-dependent coupled perturbed Hartree–Fock calculations of the hyperpolarizabilities of glycine, proline, and hydroxyproline. Two effective nonlinear dipoles are found to orient in-the-plane of the amino acids, with one of the dipoles aligning close to the pitch orientation in the triple-helix, which provides the dominant contribution to the SHG polarization properties. The calculated hyperpolarizability tensor element ratios for the collagen triple-helix models: $[(\text{Gly}_3)_n]_3$, $[(\text{Gly}-\text{Pro}_2)_n]_3$, and $[(\text{Gly}-\text{Pro}-\text{Hyp})_n]_3$, are used to predict the second-order nonlinear susceptibility ratios, $\chi_{zzz}^{(2)}/\chi_{iiz}^{(2)}$ and $\chi_{zii}^{(2)}/\chi_{iiz}^{(2)}$ of collagen fibers. From SHG microscopy polarization in, polarization out (PIPO) measurements of type I collagen in human lung tissue, a theoretical method is used to extract the triple-helix orientation angle with respect to the collagen fiber. The study shows the dominant role of amino acid orientation in the triple-helix for determining the polarization properties of SHG and provides a method for determining the triple-helix orientation angle in the collagen fibers.



INTRODUCTION

Collagen is an intriguing biological macromolecule to investigate due to its abundance, accounting for about a third of all protein in the human body, and the versatility of the structural organization with which it is found in various biological tissues.^{1,2} Networks composed of collagen, such as the extracellular matrix, are dynamic and involved in a multitude of biological processes including tissue disease (i.e., idiopathic pulmonary fibrosis^{3,4}), wound repair,⁵ and tumor development and progression.^{6–9}

There are various genetically determined types of collagen, with the most commonly investigated fibrillar collagen being type I.¹⁰ Type I collagen is composed of coiled-coil triple-helices constructed from a repeating unit Gly–X–Y, where X and Y are amino acids, most commonly proline and hydroxyproline.¹¹ Subtle differences in amino acid sequence, along with various network architectures of collagen, lead to strikingly different biomechanical properties of tissue (i.e., cornea compared to tendon).^{1,2,10,12}

There is a desire to probe and characterize the state of the three-dimensional architecture of fibrillar collagen on a submicrometer scale. Second harmonic generation (SHG) microscopy has shown promise in this endeavor.^{13–23} SHG is a nonlinear optical process whereby two photons of lower energy generate a photon of higher energy. The probability of this event occurring depends on the chemical composition and structure of the

molecules involved.²⁴ In the dipole approximation, SHG may only be generated from molecules which are noncentrosymmetric, like the collagen triple-helix. The collagen triple-helix may be reasonably approximated as possessing cylindrical symmetry (C_{6v}).^{16–23} As a result its molecular hyperpolarizability tensor β_{ijk} contains three independent elements, where ijk refers to the Cartesian components of the fields.²⁵ Kleinman symmetry further reduces this to two independent elements.^{16–18,22} In SHG microscopy, the ratios of the elements of the second-order nonlinear susceptibility tensor $\chi_{ijk}^{(2)}$ may be measured.^{13,15,18–23} The susceptibility may be thought of as the average of the molecular hyperpolarizabilities, accounting for relative orientations and local field corrections, in the focal volume.²⁶ To deduce the ratios, polarization-dependent SHG measurements are performed on aligned collagen samples, such as that found in rat-tail tendon.^{15,20,21} From the measurements, $\chi_{zzz}^{(2)}/\chi_{iiz}^{(2)}$ and $\chi_{zii}^{(2)}/\chi_{iiz}^{(2)}$ are extracted and used to characterize the collagen, where the index z corresponds to the fiber axis.

SHG polarization microscopy involves rotating the incident laser polarization with respect to the fiber axis of collagen and

Received: July 4, 2011

Revised: September 2, 2011

Published: October 4, 2011

simultaneously collecting the generated second harmonic. Additionally, an analyzer may be placed after the sample, oriented either parallel or perpendicular to the fiber axis, to differentiate the outgoing SHG polarization. For the purposes of this study, SHG polarization experiments were performed in a custom-built microscope. To improve the accuracy of determining the ratios of the elements in the nonlinear susceptibility tensor, the SHG intensity was measured at an equivalent number of analyzer and fundamental laser incident polarization angles. The corresponding plots are referred to as polarization in, polarization out (PIPO) measurements.

Understanding the microscopic organization of collagen structure is of paramount importance, and much work has been focused on the relationship between the hyperpolarizabilities of the molecules composing collagen, their relative orientations, and the second-order susceptibilities.^{16,17,19,23,27–30} There have been experimental studies focused on extracting microscopic parameters, such as estimating the packing arrangement of the fibrils¹⁶ or estimating the helical pitch angle of the collagen triple-helix from the susceptibility ratios.^{19,23} The latter estimation may be understood in terms of a formula derivation from the work of Dick,³¹ and the assumption that amino acids within the triple-helix have a dominant dipole.^{19,23,27} While the assumption is useful, its validity has been shown to be questionable for collagen.¹⁷

Deciphering the appropriate model to interpret SHG from collagen and using calculation methods to approximate its hyperpolarizability is not trivial. While quantum mechanical methods for calculating the first hyperpolarizability of molecules, such as time-dependent coupled perturbed Hartree–Fock (TDHF),^{32,33} have long existed, the computational expense of the calculation for even a small biological molecule, with a sufficient level of theory, is not practical. Therefore, approximation methods using smaller segments, which may be more readily calculated, are often employed.^{28,34,35}

For a biological macromolecule, such as collagen, it would seem natural to divide the segments into units of amino acids. Indeed, an approach has been developed to approximate biopolymers, generally with a characteristic amino acid that is used to approximate the first hyperpolarizability of all the amino acids present in the biopolymer.^{28,34} The first hyperpolarizability of the biopolymer is then taken to be the coherent summation of all the individual segments first hyperpolarizabilities. This method has its roots from the late 1970s, when approximating the first hyperpolarizability of molecules from bonds was first proposed.^{36–38} The bond additivity model, which was successful for linear polarizability and second hyperpolarizability calculations, was shown to be insufficient for approximating the first hyperpolarizability.³⁶ Instead, a method involving dividing the molecule into separate polarizable groups was recommended, with improved results.^{36,38} To adequately account for the bond–bond interactions, larger polarizable segments were utilized.

In this article, the subtleties of this approach are investigated and presented, as are the important factors to consider when approximating the first hyperpolarizability of collagen models. Ab initio calculations are presented on model collagen triple-helices, as well as the most common amino acid sequence found in type I collagen (Gly–Pro–Hyp).¹¹ The ab initio calculations suggest that amino acids do not have a sufficiently dominant dipole, as was previously assumed in estimating the helical pitch angle of collagen.^{19,23} Therefore, an alternative method for extracting microscopic properties, such as β_{zzz}/β_{iiz} , β_{zii}/β_{iiz} ,

and the orientation angle of the triple-helix axis with respect to the fiber axis from the second-order susceptibility ratios, is proposed. The incoming and outgoing SHG polarization dependence of type I collagen contained in thin lung tissue is investigated using PIPO microscopy. Susceptibility ratios are interpreted in light of the aforementioned method and the ab initio calculations.

MATERIALS AND METHODS

Calculation of the First Hyperpolarizability Tensor. Ab initio calculation of the full hyperpolarizability tensor is performed with the computational chemistry package GAMESSUS.³⁹ The time-dependent coupled perturbed Hartree–Fock (TDHF) method was employed.^{32,33} The molecular coordinates were extracted from files contained in the Protein Databank (PDB),^{40,41} with all hydrogen atom positions being geometrically optimized, without symmetry restrictions, at the DFT/B3LYP level using the 6-311++G** basis set. Restricted Hartree–Fock was used for the calculation of the nonlinear optical properties, with a basis set of RHF/6-311++G**. The following convergence parameters were used: ICUT=20, ITOL=30, INTTYP=HONDO, NCONV=7, ATOL=1.0D-0.7, BTOL=1.0D-0.7. All hyperpolarizability calculations were performed at a wavelength of 1028 nm.

The collagen-like models studied were $[(\text{Gly}_3)_n]_3$, $[(\text{Gly}-\text{Pro}_2)_n]_3$, and $[(\text{Gly}-\text{Pro}-\text{Hyp})_n]_3$, which correspond to the PDB files 2G66 (with pyrrolidine rings removed), 1K6F, and 2G66, respectively.^{40,41} The $[(\text{Gly}_3)_n]$ model was constructed by using the atomic positions given in 2G66 with all pyrrolidine rings removed, thus leaving a glycine backbone structure. The PDB file 2G66 was also used for the $[(\text{Gly}-\text{Pro}-\text{Hyp})_n]_3$ model; however, it contained 3(S)-hydroxyproline in the X position. Therefore, to obtain a $[(\text{Gly}-\text{Pro}-\text{Hyp})_n]_3$ model, all the 3(S)-hydroxyproline was replaced with proline, by the substitution of hydrogen for the additional oxygen. For the calculation of the hyperpolarizability tensor of the effective amino acids, each effective amino acid was segmented out from one of the models, and hydrogen was added. The hydrogen positions were geometrically optimized and the hyperpolarizability tensor calculated using the same parameters stated above.

To approximate the hyperpolarizability tensor of the collagen triple-helix models, the interacting segment method was employed.^{36,38} The models were segmented into polarizable units containing 3–5 amino acids, depending on the collagen model. The hydrogen positions were optimized and the hyperpolarizability tensor was calculated for each unit. Once all the units were calculated, the tensors were coherently summed, accounting for relative orientations.

The effect of segmentation on the approximation method was investigated, with segmentation at the C–C_α bond being selected, as it introduced the least error compared to N–C bond segmentation and allowed for the implementation of an interaction factor, not possible with the C_α atom segmentation. The C_α atom segmentation of, for example C–C_α–N, requires the introduction of an additional C_α atom, resulting in the bonds C–C_α and C_α–N. As was alluded to, further improvement of the approximation was achieved with the introduction of an interaction factor.³⁸ This was found to reduce the error dramatically for the test cases studied. The interaction factor accounts for the effect on the hyperpolarizability due to the interaction

between electronic transition densities of the segmented polarizable units, when the units are in close proximity to each other. Nearest-neighbor interactions between polarizable units were found to be adequate for the determination of the interaction factor. The interaction factor, it is important to note, accounts for the interactions between pairs of amino acids, while taking care not to double-count the individual amino acids' contributions. For example, consider the repeating sequence: [Gly—Pro—Hyp]_n. The hyperpolarizabilities of the amino acid pairs calculated would be $\beta_{\text{Gly—Pro}}$, $\beta_{\text{Pro—Hyp}}$, and $\beta_{\text{Gly—Hyp}}$. Clearly, if the pairs are coherently summed, double-counting of the amino acids' contribution will have occurred. Therefore, the contribution from the additional Gly, Pro, and Hyp are subtracted out. The difference between this resultant tensor and the tensor arising from the simple summation of the individual amino acids ($\beta_{\text{Gly}} + \beta_{\text{Pro}} + \beta_{\text{Hyp}}$) is the definition of the interaction factor. Thus, the interaction factor is just the hyperpolarizability of the interaction between amino acid pairs. The interaction factor was defined as $\beta_{ijk}^{\text{corr}} = \beta_{ijk}^{\text{unit}_1-\text{unit}_2} - (\beta_{ijk}^{\text{unit}_1} + \beta_{ijk}^{\text{unit}_2})$, where $\beta_{ijk}^{\text{unit}_1-\text{unit}_2}$, $\beta_{ijk}^{\text{unit}_1}$, and $\beta_{ijk}^{\text{unit}_2}$ are the hyperpolarizability elements for the polarizable units calculated together and calculated after segmentation, respectively, with the subscripts 1 and 2 referring to the polarizable unit. The interaction factor hyperpolarizability tensors were introduced to the coherent summation to approximate the full hyperpolarizability. Additionally, due to substantial differences in the residue configurations, the individual polarizable units were not assumed to be identical.⁴² This is due to the differences in configuration affecting the hyperpolarizability in a nontrivial manner. Therefore, each unit was calculated separately, as was each correction factor.

Visualization (Unit Sphere Representation). To visualize the first hyperpolarizability tensor, the unit sphere representation is used.³⁵ Briefly, an effective SHG dipole is defined as

$$\vec{\beta}_{\text{eff}} = \vec{\beta} : \hat{E}(\theta, \phi) \hat{E}(\theta, \phi) \quad (1)$$

where $\vec{\beta}$ is the hyperpolarizability tensor, and $\hat{E}(\theta, \phi)$ is the unit vector of the polarization of the incident electric field with polarization defined in spherical coordinates (θ, ϕ) . By sampling all possible incident polarizations defined by (θ, ϕ) , a unit sphere is mapped out. At each point (θ, ϕ) on the unit sphere surface, the corresponding $\vec{\beta}_{\text{eff}}$ glyph is plotted. Once the hyperpolarizability tensor was obtained, the effective SHG dipoles were calculated in MATLAB. The molecule of interest PDB file as well as the MATLAB (The MathWorks, Inc.) output files were converted to VTK files (Kitware, Inc.) and visualized in Paraview (Kitware, Inc.).

Collagen Samples. Collagen (type I) containing human lung tissue was obtained during video-assisted thoracoscopic apical bullectomy for spontaneous pneumothorax. Part of the resected specimen was embedded and cut at 0, 45, and 90°. The tissue was fixed in 10% neutral buffered formalin and processed into paraffin blocks. Sections 4 μm thick were cut and mounted between two microscope coverslips. The patient gave consent for use of tissue for research.

Polarization in, Polarization out (PIPO) Measurements. A multicontrast nonlinear microscope, previously described in ref 43, was altered for the PIPO measurements with a linear polarizer (Laser Components Inc.) and half-wave plate (Comar) inserted before the excitation objective and a linear polarizer (Laser Components Inc.) placed in front of the photomultiplier tube (Hamamatsu), for determination of the SHG polarization (Figure 1).

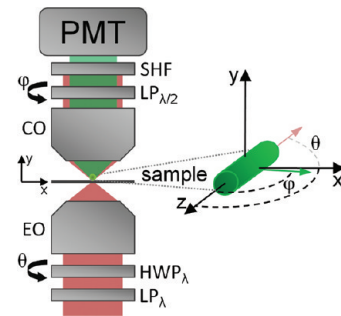


Figure 1. Polarization in, polarization out (PIPO) experimental setup: LP, linear polarizer for the fundamental λ , and second harmonic $\lambda/2$ wavelengths; HWP, half-wave plate for the fundamental λ ; EO, excitation objective; CO, collection objective; SHF, second harmonic filter; PMT, photomultiplier tube; θ and φ define the incident fundamental laser polarization and analyzer angle from the collagen fiber axis, respectively.

The microscope was coupled with a custom-built femtosecond Yb:KGd(WO₄)₂ oscillator. The 1028 nm wavelength radiation laser provided ~ 430 fs pulses at a 14.3 MHz repetition rate.⁴⁴ A 20 \times 0.75 NA air objective (Zeiss) was used for focusing the laser beam. A 514 \pm 10 nm band-pass filter (CVI Laser) was used for SHG collection. The collagen samples were imaged with ~ 30 pJ pulse energy for 50 frames at a 2 μs pixel dwell time forming an image with 128 \times 128 pixels. SHG images were collected at 100 sets of excitation and analyzer angles. The half-wave plate was rotated to 10 different evenly spaced excitation angles from $-\pi/2$ to $\pi/2$ while the analyzer was rotated to 10 different evenly spaced angles from $-\pi/2$ to $\pi/2$ for each excitation angle. A region of interest was then selected in the images and the variation in the intensity of the SHG between different images was obtained with ImageJ (National Institutes of Health) software. A contour plot was constructed in MATLAB (The Mathworks, Inc.) and fit as a function of excitation and analyzer angles with eq 13b (see Determination of the Nonlinear Susceptibility Ratio from PIPO SHG Microscopy).

THEORETICAL CALCULATIONS

Distribution of Nonlinear Dipoles in the Collagen Fibrils. With experimentally obtained susceptibility ratios and ab initio calculated hyperpolarizability values, it is possible to estimate an orientation angle of the collagen triple-helix axis relative to the fiber axis. The triple-helix is assumed to possess cylindrical symmetry (C_{6v} ; $\beta_{zzz}\beta_{zii}\beta_{izi}$),¹⁷ where the fiber is assumed to be directed along the z -axis. There is evidence that certain collagen triple-helices lie at an angle to the fiber axis.^{1,12,45,46}

If triple-helices are assumed to be oriented at an angle θ_{t-h} from the fiber axis and are evenly distributed about the fiber axis (i.e., C_{6v} symmetry is imposed on the fibers), then the corresponding susceptibility ratios can be determined (Figure 2). Defining a rotation matrix R , where angle θ_{t-h} is from the fiber axis (z -axis) and ψ is about the fiber axis (with an arbitrarily defined reference axis, perpendicular to the fiber axis),

$$R = A(\psi)B(\theta_{t-h}) = \begin{bmatrix} \cos \psi & -\sin \psi & 0 \\ \sin \psi & \cos \psi & 0 \\ 0 & 0 & 1 \end{bmatrix} \begin{bmatrix} \cos \theta_{t-h} & 0 & \sin \theta_{t-h} \\ 0 & 1 & 0 \\ -\sin \theta_{t-h} & 0 & \cos \theta_{t-h} \end{bmatrix} \quad (2)$$

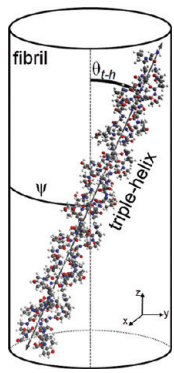


Figure 2. Depiction of the collagen triple-helix with respect to the fiber. The triple-helices are assumed to be oriented at an angle θ_{t-h} from the fiber axis and are evenly distributed about the fiber axis (z -axis). ψ is defined about the fiber axis with an arbitrarily defined reference axis (x -axis).

with the reasonable assumption that the triple-helices possess C_{6v} symmetry ($\beta_{zzz}\beta_{zii}\beta_{izi} = \beta_{iiz}$), then the rotated β_{zzz} tensor element may be represented as

$$\beta'_{zzz} = A_{zm}B_{ml}A_{zn}B_{nj}A_{zp}B_{pk}\beta_{ljk} \quad (3)$$

using Einstein's summation on repeated indexes, it follows from eq 3 and $A_{zm} = \delta_{zm}$, where δ_{zm} is the Kronecker delta, that

$$\beta'_{zzz} = B_{zl}B_{zj}B_{zk}\beta_{ljk} \quad (4)$$

Substituting and performing the summation in eq 4 yields

$$\begin{aligned} \beta'_{zzz} &= \cos \theta_{t-h}(\beta_{zzz} \cos^2 \theta_{t-h} + \beta_{zii} \sin^2 \theta_{t-h} \\ &\quad + 2\beta_{iiz} \sin^2 \theta_{t-h}) \end{aligned} \quad (5)$$

Equation 5 is independent of the angle ψ . Therefore, averaging over ψ ,

$$\chi_{zzz} = \frac{1}{2\pi} \int_0^{2\pi} \beta'_{zzz}(\psi, \theta_{t-h}) d\psi \quad (6)$$

leads to

$$\chi_{zzz} = \cos \theta_{t-h}(\beta_{zzz} \cos^2 \theta_{t-h} + \beta_{zii} \sin^2 \theta_{t-h} + 2\beta_{iiz} \sin^2 \theta_{t-h}) \quad (7)$$

Similarly,

$$\beta'_{iiz} = A_{xm}B_{ml}A_{xn}B_{nj}A_{zp}B_{pk}\beta_{ljk} \quad (8a)$$

$$\beta'_{zii} = A_{zm}B_{ml}A_{xn}B_{nj}A_{xp}B_{pk}\beta_{ljk} \quad (8b)$$

After the summation in indexes in eqs 8a and 8b and integrating as in eq 6,

$$\begin{aligned} \chi_{iiz} &= \frac{1}{2} \cos \theta_{t-h}[\beta_{zzz} \sin^2 \theta_{t-h} - \beta_{zii} \sin^2 \theta_{t-h} \\ &\quad + 2\beta_{iiz} \cos^2 \theta_{t-h}] \end{aligned} \quad (9a)$$

$$\begin{aligned} \chi_{zii} &= \frac{1}{2} \cos \theta_{t-h}[\beta_{zzz} \sin^2 \theta_{t-h} + \beta_{zii}(1 + \cos^2 \theta_{t-h}) \\ &\quad - 2\beta_{iiz} \sin^2 \theta_{t-h}] \end{aligned} \quad (9b)$$

From eqs 7 and 9, the following ratios are obtained:

$$\frac{\chi_{zzz}^{(2)}}{\chi_{iiz}^{(2)}} = \frac{2\left(2 + \frac{\beta_{zii}}{\beta_{iiz}} + \left(\frac{\beta_{zzz}}{\beta_{iiz}} - \frac{\beta_{zii}}{\beta_{iiz}} - 2\right) \cos^2 \theta_{t-h}\right)}{\frac{\beta_{zzz}}{\beta_{iiz}} - \frac{\beta_{zii}}{\beta_{iiz}} - \left(\frac{\beta_{zzz}}{\beta_{iiz}} - \frac{\beta_{zii}}{\beta_{iiz}} - 2\right) \cos^2 \theta_{t-h}} \quad (10a)$$

$$\frac{\chi_{zii}^{(2)}}{\chi_{iiz}^{(2)}} = \frac{\frac{\beta_{zzz}}{\beta_{iiz}} + \frac{\beta_{zii}}{\beta_{iiz}} - 2 - \left(\frac{\beta_{zzz}}{\beta_{iiz}} - \frac{\beta_{zii}}{\beta_{iiz}} - 2\right) \cos^2 \theta_{t-h}}{\frac{\beta_{zzz}}{\beta_{iiz}} - \frac{\beta_{zii}}{\beta_{iiz}} - \left(\frac{\beta_{zzz}}{\beta_{iiz}} - \frac{\beta_{zii}}{\beta_{iiz}} - 2\right) \cos^2 \theta_{t-h}} \quad (10b)$$

If Kleinman symmetry is imposed,^{16–18,22} the following relationship holds:

$$\cos^2 \theta_{t-h} = \frac{\frac{\chi_{zzz}^{(2)}}{\chi_{iiz}^{(2)}} \left(1 - \frac{\beta_{zzz}}{\beta_{iiz}}\right) + 6}{\left(\frac{\chi_{zzz}^{(2)}}{\chi_{iiz}^{(2)}} + 2\right) \left(3 - \frac{\beta_{zzz}}{\beta_{iiz}}\right)} \quad (11)$$

Determination of the Nonlinear Susceptibility Ratio from PIPO SHG Microscopy. To obtain an equation for the SHG intensity dependence on incoming and outgoing polarization, the collagen fiber was assumed to possess cylindrical symmetry (C_{6v} ; $\chi_{zzz}^{(2)}, \chi_{zii}^{(2)}, \chi_{iiz}^{(2)}$).^{16–23} If the effect of birefringence is negligible, as it is in the case of thin collagen samples,²² then the second harmonic electric field may be expressed as

$$\begin{bmatrix} E_{2\omega, i} \\ E_{2\omega, z} \end{bmatrix} \propto \begin{bmatrix} 2\chi_{iiz}^{(2)} E_{\omega, i} E_{\omega, z} \\ \chi_{zii}^{(2)} E_{\omega, i}^2 + \chi_{zzz}^{(2)} E_{\omega, z}^2 \end{bmatrix} \quad (12)$$

where $E_{\omega, i}$ and $E_{\omega, z}$ are the fundamental electric fields along the i - and z -axes. Substituting $E_{\omega, i} = A \sin \theta$ and $E_{\omega, z} = A \cos \theta$, where A is the electric field amplitude and θ is the angle between the incident polarization and the z -axis. When the Jones matrix formalism for an analyzer is used, the following intensity dependence on excitation, θ , and analyzer, φ , angles is established (with both angles defined from the z -axis):

$$I_{2\omega} \propto \left| \begin{bmatrix} \sin^2 \varphi & \sin \varphi \cos \varphi \\ \sin \varphi \cos \varphi & \cos^2 \varphi \end{bmatrix} \begin{bmatrix} A^2 \sin 2\theta \\ A^2 \left(\frac{\chi_{zii}^{(2)}}{\chi_{iiz}^{(2)}} \sin^2 \theta + \frac{\chi_{zzz}^{(2)}}{\chi_{iiz}^{(2)}} \cos^2 \theta \right) \end{bmatrix} \right|^2 \quad (13a)$$

$$\begin{aligned} I_{2\omega} &\propto A^2 \left[\frac{\chi_{zzz}^{(2)}}{\chi_{iiz}^{(2)}} \cos(\varphi) \cos^2(\theta) + \frac{\chi_{zii}^{(2)}}{\chi_{iiz}^{(2)}} \cos(\varphi) \sin^2(\theta) \right. \\ &\quad \left. + \sin(\varphi) \sin(2\theta) \right]^2 \end{aligned} \quad (13b)$$

RESULTS AND DISCUSSION

Ab Initio Modeling of the First Hyperpolarizability of Effective Amino Acids. The first hyperpolarizability tensors

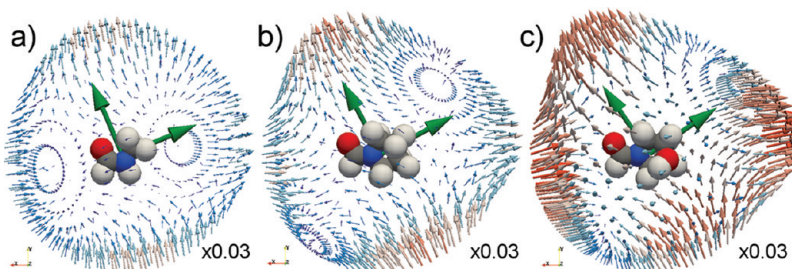


Figure 3. Visualization (Unit Sphere Representation) of the hyperpolarizability tensor of three effective amino acids: (a) glycine, (b) proline, and (c) hydroxyproline. The unit sphere vectors were scaled by $\times 0.03$, as indicated on the panels. The unit sphere representation is colored, with red being the largest magnitude effective dipoles and blue being the smallest. The atoms are colored: C, gray; O, red; N, blue; and H, white. The pitch and tilt vectors are colored green, with the pitch vector oriented parallel and the tilt vector perpendicular to the $C_\alpha NC$ backbone, respectively.

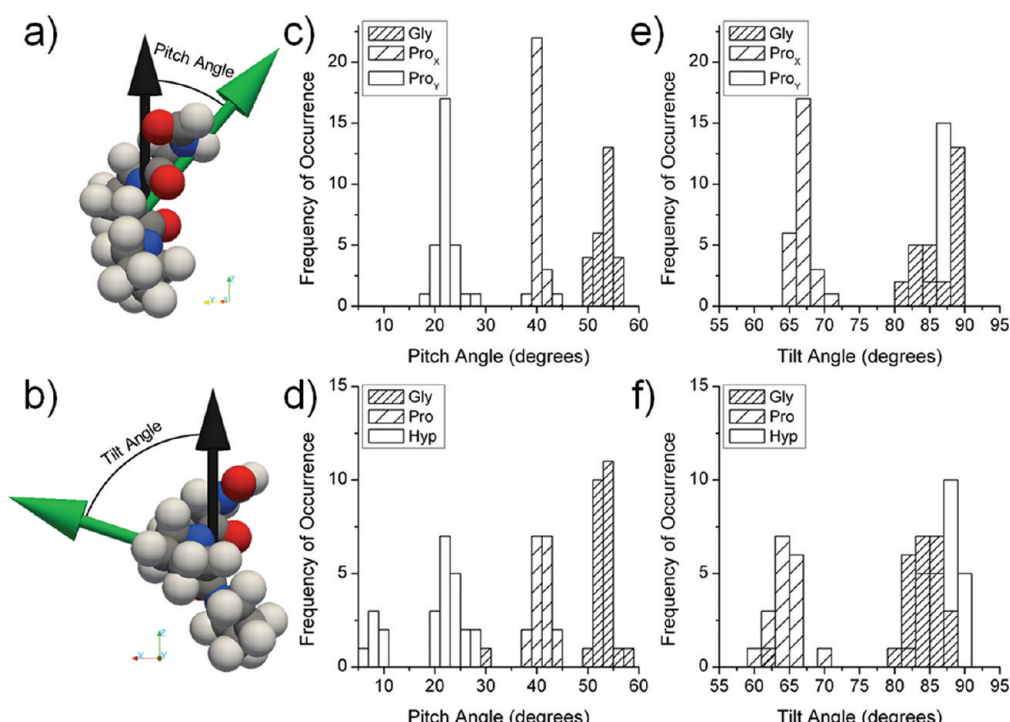


Figure 4. (a, b) Pitch and tilt vectors (green vectors) of Pro_X in the polarizable unit ($Gly-Pro_2$). The pitch and tilt angles were defined as the angle between the pitch vector (green vector) and the helical axis (black vector) of the models and the tilt vector (green vector) and the helical axis (black vector), respectively. The pitch and tilt angle distributions of the effective amino acids are shown for the models $[(Gly-Pro_2)_n]_3$ (c, e) and $[(Gly-Pro-Hyp)_n]_3$ (d, f), respectively. For the $[(Gly-Pro_2)_n]_3$ model, the prolines in the X, Y positions are labeled Pro_X and Pro_Y , respectively.

of three collagen models, extracted and modified (see Calculation of the First Hyperpolarizability Tensor) from the Protein Databank (1K6F, 2G66):^{40,41} $[(Gly_3)_n]_3$, $[(Gly-Pro_2)_n]_3$, and $[(Gly-Pro-Hyp)_n]_3$ were used to model polarization-dependent SHG. Initially, the second-order nonlinear optical properties of three effective amino acids: glycine, proline and hydroxyproline, were studied. The effective amino acids are defined by the residue group, as in Tuer et al.³⁵ The effective amino acids were segmented from the models at the $C-C_\alpha$ bond, thus, leaving the peptide bond intact. Hydrogen atoms were introduced to saturate the resulting charged atoms and were subsequently geometrically optimized. From the unit sphere representations (Figure 3), two preferential incident polarization orientations are observed for the effective amino acids.

Intuitively, this may be thought of as two SHG dipoles of the effective amino acids. Surprisingly, the orientations of the dipoles do not vary substantially between the three amino acids studied; rather it is simply the strength of the dipoles (indicated by the length and color of the glyphs in Figure 3) that change with the addition or removal of the pyrrolidine rings as the residual group. However, in general, when changing the residual group one should not expect a similar distribution to that of glycine.

For the special cases of glycine, proline, and hydroxyproline the dipoles orient approximately in-the-plane of the molecule, roughly defined by the $C_\alpha NCO$ backbone, with one dipole along the $N-C$ bond and the other approximately perpendicular to it. A molecular plane for each effective amino acid was defined, with the normal to the plane being $\hat{n} = NC_\alpha \times NC$, where NC_α and NC are unit vectors between the nitrogen- α -carbon and

nitrogen–carboxylic carbon, respectively. Unit pitch vectors and tilt vectors (Figure 3, green vectors), were defined $\hat{p} = CC_{\alpha}$ and $\hat{t} = \hat{n} \times \hat{p}$, respectively, with the CC_{α} vector being between the carboxylic carbon– α -carbon. The SHG dipoles are slightly out-of-plane for hydroxyproline, likely due to the presence of additional oxygen on the pyrrolidine ring. Glycine generates the weakest second harmonic when compared to proline and hydroxyproline, which both possess pyrrolidine rings.

The orientation of the SHG dipoles within the triple-helices, in the context of the effective amino acids' molecular plane, was

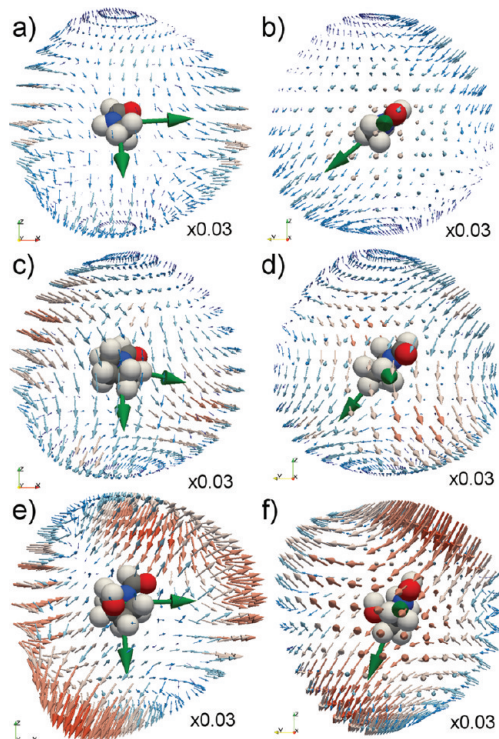


Figure 5. W Visualization (Unit Sphere Representation) of the hyperpolarizability tensor of (a, b) glycine, (c, d) proline, and (e, f) hydroxyproline at characteristic orientation along the helical axis. Two perpendicular orientations with xz (a, c, e) and yz (b, d, f) planes within the page are shown. The orientation of the unit spheres is indicated by the Cartesian coordinate axes on the panels. The effective amino acids were segmented out of the models. The unit sphere vectors were scaled by $\times 0.03$, as indicated on the panels. Coloring is the same as in Figure 1. The pitch and tilt vectors are the same as in Figure 1. A movie showing rotation of the effective amino acids unit sphere representations about the helical axis is available.

investigated. The pitch angles and tilt angles were defined as the angles between the pitch vector and the helical axis, and tilt vector and helical axis, respectively (Figure 4). The angle distributions for all effective amino acids present in the $[(\text{Gly-Pro}_{2})_n]_3$ and $[(\text{Gly-Pro-Hyp})_n]_3$ models are presented in Figure 4. The results clearly convey that the angle distribution for these models depend on the position of the effective amino acids in the helix. For both models with a repeating unit $\text{Gly}-X-Y$, the pitch angles for X are approximately between 35 and 45° , while the pitch angles for Y are between 0 and 30° . For the $[(\text{Gly-Pro})_n]_3$ model, the prolines in the X, Y positions are labeled Pro_X and Pro_Y , respectively. The glycines are found to have a pitch angle centered about 55° for both models. The angle dependence on position is likely required for the formation of stable triple-helices.

The pitch vector approximately corresponds to the SHG dipole lying parallel to the $C_{\alpha}\text{NC}$ backbone. The tilt vector, which corresponds to the other SHG dipole, is also position-dependent. Figure 5 shows characteristic orientations for the effective amino acids within the triple-helix. The SHG dipoles of glycine and hydroxyproline, oriented along the tilt vector (green vector oriented perpendicular to $C_{\alpha}\text{NC}$ backbone), clearly lie close to the x -axis, which is perpendicular to the helical axis (z -axis; Figure 5a,e). Due to the restriction of cylindrical symmetry, only the SHG dipole oriented along the pitch vector (green vector oriented parallel to $C_{\alpha}\text{NC}$ backbone), for glycine and hydroxyproline, contributes substantially to the SHG properties of the triple-helix (Figure 5b,f). For proline, both dipoles contribute to the SHG properties of the triple-helix (Figure 5c,d).

Imposing cylindrical symmetry (C_{6v}) on the effective amino acids is enlightening. This allows for the visualization of the contribution from the tensor elements, which survive the restriction ($\beta_{zzz}\beta_{zii}\beta_{izi} = \beta_{iiz}$), where due to averaging about the z -axis, the contribution from the tensor elements with x or y , arising an odd number of times, in the index vanishes (Figure 6).

Visualizing only the terms in the hyperpolarizability tensor, which persist under cylindrical symmetry, highlights the effective amino acids' contribution to the SHG originating from a collagen triple-helix. The glycine and proline effective amino acids, after imposing cylindrical symmetry, possess the following properties: $\beta_{zii} < 0 < \beta_{zzz}$ characterized by downward oriented dipole at the equator for β_{zii} and upward oriented dipoles at the poles for β_{zzz} (Figure 6a,b), where the sign is in relation to the positive z -axis. Therefore, the corresponding ratio is small in amplitude and negative, $-1 < \beta_{zzz}/\beta_{zii} < 0$. The positive β_{zzz} component, after imposing cylindrical symmetry, appears due to positive β_{zzz}

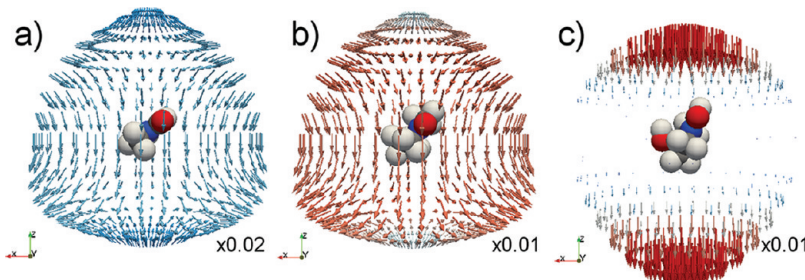


Figure 6. Visualization (Unit Sphere Representation) of the hyperpolarizability tensor of (a) glycine, (b) proline, and (c) hydroxyproline with cylindrical symmetry imposed about the helical axis. The effective amino acids were segmented out of the models. The unit sphere vectors were scaled by $\times 0.02$ for glycine and by $\times 0.01$ for proline and hydroxyproline, as indicated on the panels. Coloring is the same as in Figure 1.

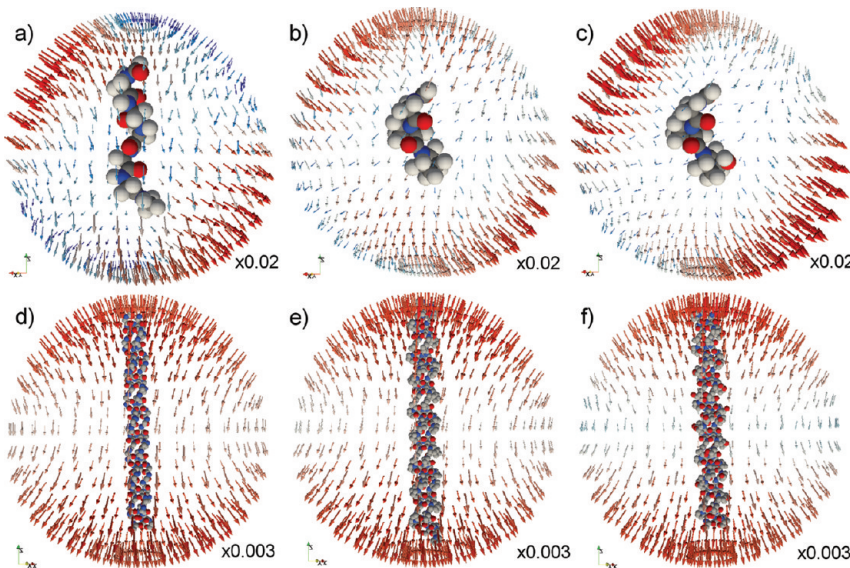


Figure 7. Visualization (Unit Sphere Representation) of the hyperpolarizability tensors of polarizable units, (a) (Gly_5), (b) $\text{Gly}-\text{Pro}_2$, and (c) $\text{Gly}-\text{Pro}-\text{Hyp}$, and the collagen models, (d) $[(\text{Gly}_5)_n]^3$, (e) $[(\text{Gly}-\text{Pro}_2)_n]^3$, and (f) $[(\text{Gly}-\text{Pro}-\text{Hyp})_n]^3$. The unit sphere vectors were scaled by $\times 0.02$ and $\times 0.003$ for the polarizable units and models, respectively, as indicated on the panels. Coloring is the same as in Figure 1.

values for the original effective amino acids (Figure 5a–d). Similarly, β_{zii} is negative due to the β_{zii} of the original effective amino acids, which arises due to the presence of the SHG dipoles oriented along the pitch vector. Additionally, for proline, the SHG dipole oriented along the tilt vector contributes to the β_{zii} component, making its magnitude much larger than for glycine.

The angles at which the pitch and tilt vectors of the effective amino acid, hydroxyproline, orient with respect to the helical axis is small and yields a unit sphere distribution, which corresponds to a simple dipole, with the following properties: $\beta_{zii} \approx 0$ and β_{zzz} being large and negative (Figure 6c). For hydroxyproline, the ratio β_{zzz}/β_{iiz} is large, though the sign is uncertain, as β_{zii} is close to 0 and may be positive or negative.

The β_{zzz} when all three effective amino acids are coherently summed is negative, implying the β_{zzz} contribution from hydroxyproline dominates over glycine and proline, while the β_{zii} of glycine and proline dominates over hydroxyproline. Overall, the contribution from glycine was found to be less substantial than the other effective amino acids' contribution (Figure 6), validating that the N–C bonds are not the dominate source of second harmonic in the triple-helix.^{20,47,48} While the N–C bond is along the pitch vector, it is the addition of the C–H bonds in the pyrrolidine rings (Figure 6b), which lead to a substantial increase in the magnitude of the SHG dipole parallel to the pitch vector.

Sum frequency generation-vibrational studies on type I collagen fibers found that the achiral second harmonic originates from CH_2 groups.⁴⁸ This explains the large SHG dipoles from proline and hydroxyproline compared to glycine (Figures 3 and 6). The calculations confirm that the most likely contributor to achiral SHG is from the methylene functional group in the pyrrolidine rings, previously suggested by Rocha-Mendoza et al.⁴⁸ Effective amino acids with different residues will complicate this explanation as the SHG dipole distribution will correspondingly vary.

From the models it is interesting to note that the amplitude of effective SHG dipoles is largest when the incident polarization is coparallel with the helical pitch, as suggested previously.^{19,23,27} In the previous work, the pitch vector is oriented along the

angle $\theta_p = \arctan(2\pi R/P)$ to the z -axis, where R and P are the radius and pitch height of a single helix,^{19,23} However, this is not strictly true as the triple-helices may also be oriented at an angle to the collagen fiber axis. Calculations of the triple-helix orientation angle with respect to the collagen fiber will be presented in a later section, Triple-Helix Orientation Angle in Collagen Fiber.

Knowing both the angle distributions and the tensor elements, which persist under cylindrical symmetry for each effective amino acid, an approximation of β_{zzz}/β_{iiz} for the triple-helix is possible. When the calculation is performed, a ratio of ~ 0.6 is determined, which is lower than that expected from the collagen triple-helix. Determining the ratio from a single effective amino acid, glycine, proline, or hydroxyproline, yields even more unrealistic results, such as a negative ratio (glycine and proline) or an extremely large ratio (hydroxyproline). Thus, the utilization of all three effective amino acids improves the ratio approximation and aids in qualitatively understanding its origin.

Ab Initio Modeling of the Triple-Helix First Hyperpolarizability. To improve the β_{zzz}/β_{iiz} ratio approximation quantitatively, a more refined strategy is required. For the approximation of the triple-helix models, the larger the polarizable units are in terms of number of atoms used, the more accurate the approximation will be to the full calculation since more interactions between atoms will be taken into account. The polarizable units are the molecules segmented from the models and represent the building blocks of the approximation. Calculating single effective amino acids was shown to be less than ideal, while calculating the full triple-helix is not feasible due to computational restrictions. Thus, a trade-off was made and each model was segmented into polarizable units containing 3–5 amino acids (Figure 7a–c).

The polarizable units (Gly_5 , $\text{Gly}-\text{Pro}_2$, and $\text{Gly}-\text{Pro}-\text{Hyp}$) all contain dipole distributions of comparable amplitude, which is reasonable as each unit is composed of a similar number of atoms. The SHG dipoles of the $\text{Gly}-\text{Pro}-\text{Hyp}$ unit are slightly larger in magnitude.

Table 1. Percentage Difference for Hyperpolarizability Approximation Resulting from Segmentation of C–C_α, N–C or C_α^a

polarizable unit	C–C _α		N–C		C _α
	with	without	with	without	
	corr.	corr.	corr.	corr.	
Gly ₃	4 ± 6%	9 ± 16%	8 ± 12%	24 ± 28%	10 ± 12%
Gly–Pro ₂	1 ± 4%	15 ± 28%			
Gly–Pro–Hyp	1 ± 2%	11 ± 22%			

^a See Ab Initio Modeling of the Triple-helix First Hyperpolarizability for information on the percent difference calculation.

The unit sphere distributions of the polarizable units are somewhat complicated. The distribution of SHG dipole orientations is vaguely characteristic of cylindrical symmetry. However, the variation in amplitudes distorts this observation and leads to the distributions appearing to be more characteristic of a dipole oriented along the helical pitch. As the number of effective amino acids in the polarizable units increase, the dipole distributions will tend closer to resembling perfect cylindrical symmetry.

The effect of segmentation on the triple-helix approximation method was investigated with a Gly₃ polarizable unit. The reported percent difference, summarized in Table 1, is defined as $\mu \pm 2\sigma$, where μ is the average percent difference of the tensor elements and σ is the standard deviation. The percent difference of the tensor elements was defined as $|(\beta_{ijk}^{\text{full}} - \beta_{ijk}^{\text{approx}})/\Sigma_i \beta_{ijk}^{\text{full}}|$, where $\beta_{ijk}^{\text{approx}}$ is the hyperpolarizability element determined by the interacting segment method (with interaction factors included when applicable) and $\beta_{ijk}^{\text{full}}$ is the element found by the full ab initio calculation with no segmentation. As a result of investigating the Gly₃ unit, truncation at the C–C_α bond was found to produce the lowest mean percent difference (9 ± 16%) compared to truncation at the C_α–N bond (24 ± 28%). Welch's *t* test of unequal variance finds with 95% confidence the mean of C_α–N to be larger than C–C_α by 6.4 to 22.5%. Segmentation at the C_α–N bond results in the worst approximation, which is reasonable given that the truncation disrupts an asymmetric bond. Statistically, C–C_α bond truncation and the C_α atom (10 ± 12%) truncation are equivalent. For clarity, an example C_α atom truncation of the molecule, C–C_α–N, would result in two units; C–C_α and C_α–N. Hence, this method leads to the number of C_α atoms increasing linearly with the number of segmentations.

Truncation at the C–C_α bond was utilized, as it allowed for a further improvement to the approximation by the introduction of an interaction factor. A consideration in the approximation of an interaction factor is the effect of the presence of additional hydrogen at the truncation points. To determine the magnitude of the first hyperpolarizability of a C–H bond, CH₄ was calculated and decomposed into four dipoles oriented parallel to the bond axes. The first hyperpolarizability of the C–H bond was determined to be on the order of ~30 au. This result revealed the sensitivity of the first hyperpolarizability calculation to hydrogen positioning.

If the bond additivity model is assumed to be valid then the appropriate interaction factor due to segmentation would simply be the subtraction of the contribution from the two additional C–H bonds, because the symmetric C–C bond would have no impact on SHG. In general, the additional C–H bonds tend to orient antiparallel; thus, the resulting interaction factor is null.

Therefore, the first approximation of the interaction factor employing the bond additivity model is clearly insufficient.

Just as the interacting segment method (which is an improvement over the bond additivity model) accounts for bond–bond interactions, similar considerations must be made for the interaction factor between polarizable pairs. The interaction factor should account for the interaction between electronic transition densities of the segmented polarizable units when the units are in close proximity to each other. The change in the electronic transition density due to the segmentation must be approximated and its effect on the first hyperpolarizability calculated. To this end, nearest-neighbors were found to be sufficient in determining the interaction factor due to changes in the electronic transition density. As an example, consider the sequence [Gly–Pro–Hyp]_n discussed in Calculation of the First Hyperpolarizability Tensor, where the polarizable units are Gly–Pro, Pro–Hyp, and Gly–Hyp. The hyperpolarizability of this sequence is $\beta_{\text{Gly-Pro}} + \beta_{\text{Pro-Hyp}} + \beta_{\text{Gly-Hyp}} - (\beta_{\text{Gly}} + \beta_{\text{Pro}} + \beta_{\text{Hyp}})$. ($\beta_{\text{Gly}} + \beta_{\text{Pro}} + \beta_{\text{Hyp}}$) is subtracted out so as not to double-count the amino acids' contribution. The interaction factor, β_{int} , is the difference between the hyperpolarizability of the sequence and the individual amino acids' contributions: $\beta_{\text{int}} = \beta_{\text{Gly-Pro}} + \beta_{\text{Pro-Hyp}} + \beta_{\text{Gly-Hyp}} - 2(\beta_{\text{Gly}} + \beta_{\text{Pro}} + \beta_{\text{Hyp}})$.

The procedure of calculating pairs of amino acids, including the interaction factor, and then accounting for double-counting was found to reduce the percent difference dramatically for the test cases studies (Table 1), especially for the Gly–Pro₂ (15 ± 28% to 1 ± 4%) and Gly–Pro–Hyp (11 ± 22% to 1 ± 2%) units.

When the interaction factors are included for the Gly–Pro–Hyp discussed in Ab Initio Modeling of the First Hyperpolarizability of Effective Amino Acids and cylindrical symmetry is imposed, a much more agreeable β_{zzz}/β_{iiz} of ~1.4 is obtained.

Though not attempted in this study, it should be noted that additional correction factors are likely necessary due to the presence of the effective amino acid electronic transition densities, at relatively close distances, in adjacent chains of the triple-helix.

After calculation of each polarizable unit and the corresponding interaction factors between polarizable pairs, the calculated hyperpolarizability tensors of all the units and interaction factors were coherently summed, accounting for relative orientations. The resultant tensors were visualized with the Unit Sphere Representation (Figure 7d–f).

The collagen triple-helix models are all similar qualitatively, clearly displaying cylindrical symmetry. Quantitatively the [(Gly₃)₃], [(Gly–Pro₂)₃], and [(Gly–Pro–Hyp)₃] model's hyperpolarizability ratios ($\beta_{zii}/\beta_{iiz}, \beta_{zzz}/\beta_{iiz}$) were (0.97, 1.32), (0.98, 1.51), and (0.97, 1.79), respectively. The models of the hyperpolarizability suggest that $\beta_{zii}/\beta_{iiz} \approx 1$, which implies from eqs 10 that Kleinman symmetry holds for the second-order susceptibility of collagen at 1028 nm.

Comparing the results of the approximation with Hyper-Rayleigh scattering measurements performed at 790 nm on type I collagen and a [(Gly–Pro₂)₃] polypeptide, revealed the effectiveness of the approximation. Experimental estimates of β_{zzz}/β_{iiz} for rat-tail tendon type I collagen was obtained by Deniset-Besseau et al. and found to be $1.1 \leq \beta_{zzz}/\beta_{iiz} \leq 2.0$.¹⁷ All the models fall well within the experimentally determined range for type I. In the same study, a [(Gly–Pro₂)₃] model was investigated and an experimental range of $1.4 \leq \beta_{zzz}/\beta_{iiz} \leq 5.0$ was determined.¹⁷ The approximation of [(Gly–Pro₂)₃] falls

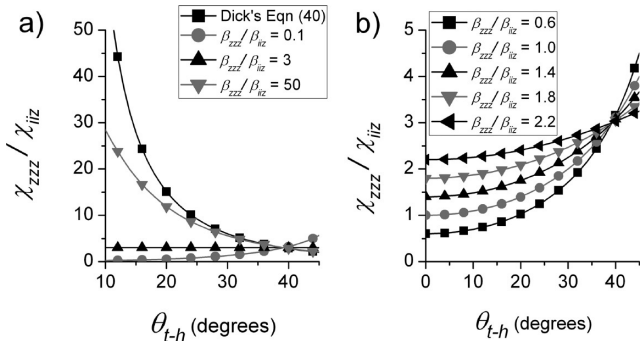


Figure 8. (a) Plots of $\chi_{zzz}^{(2)}/\chi_{iiz}^{(2)}$ as a function of angle from the helical axis, θ_{t-h} , at fixed β_{zzz}/β_{iiz} values: 0.1 (gray circle), 3 (black triangle), 50 (gray triangle), ∞ (Dick's eq 40,²³ black square). (b) Plots of $\chi_{zzz}^{(2)}/\chi_{iiz}^{(2)}$ as a function of angle from the helical axis, θ_{t-h} , at relevant β_{zzz}/β_{iiz} values for collagen: 0.6 (black square), 1.0 (gray circle), 1.4 (black triangle-up), 1.8 (gray triangle-down), 2.2 (black triangle-side).

within these experimentally determined bounds, which gives credence to the usefulness of the approximation method.

An average hyperpolarizability value for the $[(\text{Gly}-\text{Pro}_2)_n]_3$ model at 800 nm has previously been presented, without interaction factors, by Tuer et al.³⁵ An order of magnitude agreement of the calculated susceptibility values with the experiment has been found, although, in the approximation solvent effects, electron correlations, polarizable unit interactions, and possible resonance enhancements were neglected. If resonance enhancement was appreciable at the measured wavelength, the perturbation approximation method utilized in TDHF would no longer be valid.

Our results are consistent with the research of Deniset-Besseau et al.,¹⁷ where it was pointed out that, although each amino acid is not a strong harmonophore, coherent addition of radiation from many well-aligned nonlinear emitters in the collagen triple-helix results in the strong SHG signal. The study also showed that the β_{zii} of the triple-helix is not negligible compared to β_{zzz} , which is confirmed in our investigations. Deniset-Besseau and co-workers intuitively suggested that, if all the collagen molecules are aligned in the same direction within the fibrils, the second-order susceptibility should reflect the hyperpolarizability. Notably, the ratio of the susceptibility should be similar to the ratio of the hyperpolarizability.

Triple-Helix Orientation Angle in Collagen Fiber. An increasingly popular technique for characterizing the pitch of collagen utilizes a formula relating $\chi_{zzz}^{(2)}/\chi_{iiz}^{(2)}$ to an orientation angle of a dipole, $\langle \cos^2 \theta \rangle = 2/((\chi_{zzz}^{(2)}/\chi_{zxx}^{(2)}) + 2)$, as was first derived by Dick (eq 40 in ref 31). While popular, care should be taken in determining whether the initial assumptions are satisfied before its implementation. For example, a dominant dipole for the molecules is assumed, which is clearly not the case for the effective amino acids studied (Figure 3).¹⁷ While it appears reasonable to assume an effective dipole along the helical pitch (Figures 5 and 6), the effective dipole was found not to be dominant enough to utilize Dick's formula, unless the orientation angle is near or above the magic angle ($\sim 39^\circ$; see Figure 8a).

Thus, while Dick's initial conditions are not satisfied, the method may still be implemented with moderate success for collagen, since the effective dipoles lie approximately along the helical pitch.

The possibility of relating the hyperpolarizability ratios, second-order susceptibility ratios, and the orientation angle of the

triple-helices is also of interest. Therefore, a method is proposed relating the triple-helices orientation to the fiber axis. The triple-helices are assumed to possess cylindrical symmetry (C_{6v}) and be evenly distributed about the fiber axis. Figure 8 plots $\chi_{zzz}^{(2)}/\chi_{iiz}^{(2)}$ as a function of θ_{t-h} at fixed β_{zzz}/β_{iiz} values. The plots confirm the importance of having a dominant dipole when utilizing Dick's special eq 40 for a dominant β_{zzz} .³¹

From Figure 8a, it is clear that even when $\beta_{zzz}/\beta_{iiz} = 50$ the susceptibility is only reasonably approximated by Dick's special case above an orientation angle of $\sim 25^\circ$. As the orientation angle tends to zero, Dick's equation tends to infinity, while eq 10a tends to β_{zzz}/β_{iiz} . Interestingly, there is a critical value at $\beta_{zzz}/\beta_{iiz} = 3$ in the function described by eq 10a, revealing that if $\beta_{zzz}/\beta_{iiz} < 3$, the susceptibility ratio increases with increasing orientation angle, which is counter to what would be expected from a simple dipole.

The hyperpolarizability ratios close to what is expected from the collagen triple-helix were investigated (Figure 8b). The plot suggests that while the hyperpolarizability ratio for the collagen triple-helix may be constant for various tissues, the second-order nonlinear susceptibility ratios may vary depending on the orientation angle between the triple-helix and the fiber axis. If the collagen triple-helices are aligned straight in relation to the fibril axis then $\chi_{zzz}^{(2)}/\chi_{zii}^{(2)}$ should be similar to β_{zzz}/β_{zii} . This suggests that a type I collagen sample, like rat-tail tendon, with a $\theta_{t-h} = 5^\circ$ is a good indication of β_{zzz}/β_{zii} . Orientations where the collagen triple-helices are at large angles would produce large $\chi_{zzz}^{(2)}/\chi_{zii}^{(2)}$ ratios. Indeed, the collagen triple-helix monomer has been found to orient at various angles relative to the fiber axis.^{1,2,12,45,46} Angles as large as 18° have been reported for collagen in interstitial tissues and cornea.¹

To predict susceptibility ratios for "straight" fibrils, eqs 10a and 10b were used in conjunction with $\theta_{t-h} = 5^\circ$ and the $(\beta_{zii}/\beta_{iiz} = 1, \beta_{zzz}/\beta_{iiz})$ values determined from the collagen models. Depending on the model, the predicted $\chi_{zzz}^{(2)}/\chi_{iiz}^{(2)}$ ratio ranged from 1.3 to 1.9. The measured susceptibility ratios for type I collagen in "straight" tendon ranged from 1.34 to 1.47.^{13,15,21,23} Therefore, for type I collagen in tissues where the triple-helix orients at a larger angle within the fibril, higher susceptibility values can be reasonably expected. By combining the experimentally measured susceptibility ratio with the calculated hyperpolarizability ratios, an orientation angle of the triple-helices in the fiber can be obtained.

PIPO Measurements of a Thin Collagen Sample. To verify the predictions of the model, PIPO SHG microscopy measurements were performed on a thin section of human lung tissue containing type I collagen. A small region of interest was selected with parallel fibers showing low curvature (Figure 9a) and the PIPO measurements were performed. The experimental PIPO contour plot was constructed from the 10×10 SHG intensity data set with different fundamental polarization and analyzer angles. A linear interpolation algorithm was used to generate the surface (Figure 9b). The intensity data set was subsequently fit with eq 13 and its contour plot generated (Figure 9c).

Initially, the susceptibility ratios were determined to be $\chi_{zzz}^{(2)}/\chi_{iiz}^{(2)} = 1.8 \pm 0.1$ and $\chi_{zii}^{(2)}/\chi_{iiz}^{(2)} = 0.9 \pm 0.1$. From the collagen model hyperpolarizability approximations, Kleinman symmetry is expected to hold. If Kleinman symmetry is imposed on the fit, the corresponding susceptibility ratio is then $\chi_{zzz}^{(2)}/\chi_{iiz}^{(2)} = 1.9 \pm 0.1$, with all other parameters remaining similar. With the assumption of Kleinman symmetry, the simplest explanation of the susceptibility ratio, in terms of the model

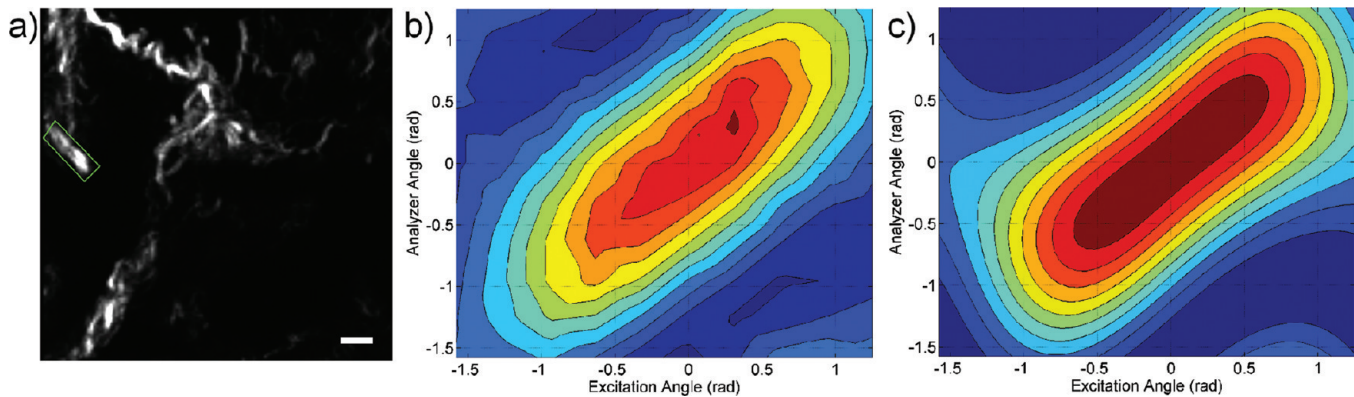


Figure 9. PIPO measurement of collagen fibers from a thin section of lung tissue. (a) Displays a cumulative 50 frame image of SHG from the collagen fibers at an arbitrary input polarization, with no output polarizer. (b and c) Experimental and fit PIPO contour plots, respectively, for the region of interest highlighted by the green box in (a). The scale bar is 15 μm .

hyperpolarizabilities, is that the region of interest of collagen is best described by the $[(\text{Gly}-\text{Pro}-\text{Hyp})_n]_3$ triple-helix model oriented at an angle of $12 \pm 8^\circ$ to the fiber axis. If the $[(\text{Gly}_3)_n]_3$ and $[(\text{Gly}-\text{Pro}_2)_n]_3$ model hyperpolarizability ratios are employed, orientation angles of $25 \pm 2^\circ$ and $21 \pm 3^\circ$ are calculated, respectively. If β_{zzz}/β_{zii} is assumed to be approximately equal to $\chi_{zzz}^{(2)}/\chi_{zii}^{(2)}$ of type I rat-tail tendon, then an orientation angle of $23.4 \pm 1.1^\circ$ is calculated. The orientation angle appears relatively insensitive to even fairly large differences in the hyperpolarizability ratio ($1.3-1.9$). Various other regions of interest, containing fibers of low curvature, were measured with the PIPO method and yielded similar susceptibility ratios. The ratios are larger than those found for type I collagen in tendon ($1.34-1.47$). However, as was stated, this does not imply a different hyperpolarizability ratio or pitch angle of the chains in the triple-helices for type I collagen in tendon relative to the triple-helices found in collagen of the lung. Instead, it is more probable that the discrepancy in susceptibility ratios is best explained by the orientation of the triple-helices themselves within the type I collagen fibrils.

An alternative explanation is that the measured susceptibility ratio is a result of fiber orientation. If the fibers are oriented at an angle to the image plane, the ratio would appear larger according to $(\chi_{zzz}^{(2)}/\chi_{zii}^{(2)})_{\text{apparent}} = (\chi_{zzz}^{(2)}/\chi_{zii}^{(2)})_{\text{true}} \cos^2 \alpha + 3 \sin^2 \alpha$, where α is the angle between the fiber and the image plane and $(\chi_{zzz}^{(2)}/\chi_{zii}^{(2)})_{\text{true}}$ is the true ratio if the fiber were oriented in the image plane.¹⁸ If a true ratio of 1.4 is assumed for the fiber then an angle of 35° is required to obtain an apparent ratio of 1.9. This is a fairly substantial angle and is unlikely to explain the apparent ratio, as the fibrils studied are visible across many micrometers in the image plane. However, both the orientation of the triple-helices within the fiber and the fiber itself likely play a role in determining the measured susceptibility ratio.

CONCLUSIONS

A simple collagen fiber model, along with first hyperpolarizability ratios of three collagen triple-helix models: $[(\text{Gly}_3)_n]_3$, $[(\text{Gly}-\text{Pro}_2)_n]_3$, and $[(\text{Gly}-\text{Pro}-\text{Hyp})_n]_3$, calculated using the time-dependent coupled perturbed Hartree-Fock method, were used to predict and interpret the second-order nonlinear susceptibility ratios, $\chi_{zzz}^{(2)}/\chi_{zii}^{(2)}$ and $\chi_{zii}^{(2)}/\chi_{zii}^{(2)}$ of fibrillar type I collagen. Ab initio calculation of the hyperpolarizabilities of glycine, proline, and hydroxyproline are used to provide an intuitive understanding of the SHG properties of the collagen

triple-helix models. The calculations revealed that the effective amino acids had SHG dipoles, which persist under the restrictions of cylindrical symmetry, oriented along the $C_\alpha\text{NC}$ backbone, thus helping to explain why maximum SHG intensity is obtained when the incident laser polarization is approximately coparallel to the helical pitch of the collagen triple-helices. This is not strictly true, as the triple-helices themselves may also be oriented at relatively small angles to the collagen fiber axis. SHG microscopy was utilized to perform PIPO measurements on collagen contained in human lung tissue, which confirmed the predicted ratios. Using the collagen triple-helix models along with PIPO measurements, the orientation of the triple-helices in a type I collagen fiber found in lung tissue was determined to be between approximately 10 and 30° with respect to the fiber axis. The ability to characterize collagen structure in various environments is promising in the pursuit of understanding numerous collagen related biological processes, such as tissue disease of idiopathic pulmonary fibrosis, wound repair, and tumor development and progression.

The authors gratefully acknowledge support by the Natural Sciences and Engineering Research Council of Canada and the Ontario Centres of Excellence, Canada Foundation for Innovation, and Ontario Innovation Trust. Computations were performed on the GPC supercomputer at the SciNet HPC Consortium. SciNet is funded by: the Canada Foundation for Innovation under the auspices of Compute Canada; the Government of Ontario; Ontario Research Fund—Research Excellence; and the University of Toronto.

ASSOCIATED CONTENT

W Web Enhanced Feature. A movie showing the rotation of the effective amino acids unit sphere representations about the helical axis.

AUTHOR INFORMATION

Corresponding Author

*Phone: (905) 828-3821. Fax: (905) 828-5425. E-mail: virgis.barzda@utoronto.ca.

REFERENCES

- Ottani, V.; Raspanti, M.; Ruggeri, A. Collagen structure and functional implications. *Micron* **2001**, *32*, 251–260.

- (2) Orgel, J. P. R. O.; San Antonio, J. D.; Antipova, O. Molecular and structural mapping of collagen fibril interactions. *Connect. Tissue Res.* **2011**, *52*, 2–17.
- (3) Strupler, M.; Pena, A.-M.; Hernest, M.; Tharaux, P.-L.; Martin, J.-L.; Beaurepaire, E.; Schanne-Klein, M.-C. Second harmonic imaging and scoring of collagen in fibrotic tissues. *Opt. Express* **2007**, *15*, 4054–4065.
- (4) Pena, A.-M.; Fabre, A.; Débarre, D.; Marchal-Somme, J.; Crestani, B.; Martin, J.-L.; Beaurepaire, E.; Schanne-Klein, M.-C. Three-dimensional investigation and scoring of extracellular matrix remodeling during lung fibrosis using multiphoton microscopy. *Microsc. Res. Tech.* **2007**, *70*, 1–9.
- (5) Albini, A.; Sporn, M. B. The tumour microenvironment as a target for chemoprevention. *Nat. Rev.* **2007**, *7*, 139–147.
- (6) Joyce, J. J. Therapeutic targeting of the tumor microenvironment. *Cancer Cell* **2005**, *7*, 513–520.
- (7) Xu, R.; Boudreau, A.; Bissell, M. J. Tissue architecture and function: dynamic reciprocity via extra- and intracellular matrices. *Cancer Metastasis Rev.* **2009**, *28*, 167–176.
- (8) Mueller, M. M.; Fusenig, N. E. Friends or foes—bipolar effects of the tumour stroma in cancer. *Nat. Rev.* **2004**, *4*, 839–849.
- (9) Brown, E.; McKee, T.; diTomaso, E.; Pluen, A.; Seed, B.; Boucher, Y.; Jain, R. K. Dynamic imaging of collagen and its modulation in tumors *in vivo* using second-harmonic generation. *Nat. Med.* **2003**, *9*, 796–800.
- (10) Shoulders, M. D.; Raines, R. T. Collagen structure and stability. *Annu. Rev. Biochem.* **2009**, *78*, 929–958.
- (11) Ramshaw, J. A. M.; Shah, N. K.; Brodsky, B. Gly–X–Y tripeptide frequencies in collagen: a context for host-guest triple-helical peptides. *J. Struct. Biol.* **1998**, *122*, 86–91.
- (12) Hulmes, D. J. S. Building collagen molecules, fibrils, and suprafibrillar structures. *J. Struct. Biol.* **2002**, *137*, 2–10.
- (13) Stoller, P.; Celliers, P. M.; Reiser, K. M.; Rubenchik, A. M. Quantitative second-harmonic generation microscopy in collagen. *Appl. Opt.* **2003**, *42*, 5209–5219.
- (14) Nadiarnykh, O.; Campagnola, P. J. Retention of polarization signatures in SHG microscopy of scattering tissues through optical clearing. *Opt. Express* **2009**, *17*, 5794–5806.
- (15) Gusachenko, I.; Latour, G.; Schanne-Klein, M.-C. Polarization-resolved second harmonic microscopy in anisotropic thick tissues. *Opt. Express* **2010**, *18*, 19339–19352.
- (16) Williams, R. M.; Zipfel, W. R.; Webb, W. W. Interpreting second-harmonic generation images of collagen I fibrils. *Biophys. J.* **2005**, *88*, 1377–1386.
- (17) Deniset-Besseau, A.; Duboisset, J.; Benichou, E.; Hache, F.; Brevet, P.-F.; Schanne-Klein, M. C. Measurement of the second-order hyperpolarizability of the collagen triple helix and determination of its physical origin. *J. Phys. Chem. B* **2009**, *113*, 13437–13445.
- (18) Erikson, A.; Örtengren, J.; Hompland, T.; Davies, C. L.; Lindgren, M. Quantification of the second-order nonlinear susceptibility of collagen I using a laser scanning microscope. *J. Biomed. Opt.* **2007**, *12* (4), 044002–(1–10).
- (19) Su, P.-J.; Chen, W.-L.; Chen, Y.-F.; Dong, C.-Y. Determination of collagen nanostructure from second-order susceptibility tensor analysis. *Biophys. J.* **2011**, *100*, 2053–2062.
- (20) Freund, I.; Deutsch, M.; Sprecher, A. Optical second-harmonic microscopy, crossed-beam summation, and small-angle scattering in rat-tail tendon. *Biophys. J.* **1986**, *50*, 693–712.
- (21) Stoller, P.; Kim, B.-M.; Rubenchik, A. M.; Reiser, K. M.; Da Silva, L. B. Polarization-dependent optical second-harmonic imaging of a rat-tail tendon. *J. Biomed. Opt.* **2002**, *7*, 205–214.
- (22) Stoller, P.; Reiser, K. M.; Celliers, P. M.; Rubenchik, A. M. Polarization-modulated second harmonic generation in collagen. *Biophys. J.* **2002**, *82*, 3330–3342.
- (23) Tiaho, F.; Recher, G.; Rouède, D. Estimation of helical angles of myosin and collagen by second harmonic generation imaging microscopy. *Opt. Express* **2007**, *15*, 12286–12295.
- (24) Buckingham, A. D.; Orr, B. J. Molecular hyperpolarizabilities. *Quart. Rev. Chem. Soc. London* **1967**, *21*, 195–212.
- (25) Boyd, R. W. *Nonlinear Optics*, 2nd ed.; Academic Press: New York, 2003; Ch. 1.
- (26) Moreaux, L.; Sandre, O.; Mertz, J. Membrane imaging by second-harmonic generation microscopy. *J. Opt. Soc. Am. B* **2000**, *17*, 1685–1694.
- (27) Plotnikov, S. V.; Millard, A. C.; Campagnola, P. J.; Mohler, W. A. Characterization of the myosin-based source for second-harmonic generation from muscle sarcomeres. *Biophys. J.* **2006**, *90*, 693–703.
- (28) Loison, C.; Simon, D. Additive model for the second harmonic generation hyperpolarizability applied to a collagen-mimicking peptide (Pro–Pro–Gly)₁₀. *J. Phys. Chem. A* **2010**, *114*, 7769–7779.
- (29) Shcheslavskiy, V. I.; Petrov, G. I.; Yakovlev, V. V. Nonlinear optical properties of collagen in solution. *Chem. Phys. Lett.* **2005**, *402*, 170–174.
- (30) Shcheslavskiy, V. I.; Saltiel, S. M.; Ivanov, D. A.; Ivanov, A. A.; Petrushevich, V. Y.; Petrov, G. I.; Yakovlev, V. V. Nonlinear optics of molecular nanostructures in solution: Assessment of the size and nonlinear optical properties. *Chem. Phys. Lett.* **2006**, *429*, 294–298.
- (31) Dick, B. Irreducible tensor analysis of sum- and difference-frequency generation in partially oriented samples. *Chem. Phys.* **1985**, *96*, 199–215.
- (32) Karna, S. P.; Dupuis, M. Frequency dependent nonlinear optical properties of molecules: formulation and implementation in the HONDO program. *J. Comput. Chem.* **1990**, *12*, 487–504.
- (33) Sekino, H.; Bartlett, R. J. Frequency dependent nonlinear optical properties of molecules. *J. Chem. Phys.* **1986**, *85*, 976–989.
- (34) Perry, J. M.; Moad, A. J.; Nathan, J. B.; Wampler, R. D.; Simpson, G. J. Electronic and vibrational second-order nonlinear optical properties of protein secondary structural motifs. *J. Phys. Chem. B* **2005**, *109*, 20009–20026.
- (35) Tuer, A.; Krouglov, S.; Cisek, R.; Tokarz, D.; Barzda, V. Three-dimensional visualization of the first hyperpolarizability tensor. *J. Comput. Chem.* **2010**, *32*, 1128–1134.
- (36) Miller, C. K.; Ward, J. F. Measurements of nonlinear optical polarizabilities for some halogenated methanes: the role of bond-bond interactions. *Phys. Rev. A* **1977**, *16*, 1179–1185.
- (37) Levine, B. F.; Bethea, C. G. Second and third order hyperpolarizabilities of organic molecules. *J. Chem. Phys.* **1975**, *63*, 2666–2682.
- (38) Sundberg, K. R. A group-dipole interaction model of the molecular polarizability and the molecular first and second hyperpolarizabilities. *J. Chem. Phys.* **1976**, *66*, 114–118.
- (39) Schmidt, M. W.; Baldridge, K. K.; Boatz, J. A.; Elbert, S. T.; Gordon, M. S.; Jensen, J. H.; Kosecki, S.; Matsunaga, N.; Nguyen, K. A.; Su, S. J.; Windus, T. L.; Dupuis, M.; Montgomery, J. A. General atomic and molecular electronic structure system. *J. Comput. Chem.* **1993**, *14*, 1347–1363.
- (40) Schumacher, M. A.; Mizuno, K.; Bachinger, H. P. The crystal structure of a collagen-like polypeptide with 3(s)-hydroxyproline residues in the Xaa position forms a standard 7/2 collagen triple helix. *J. Biol. Chem.* **2006**, *281*, 27566–27574.
- (41) Berisio, R.; Vitagliano, L.; Mazzarella, L.; Zagari, A. Crystal structure of the collagen triple helix model [(Pro–Pro–Gly)(10)][3]. *Protein Sci.* **2002**, *11*, 262–270.
- (42) Hovmöller, S.; Zhou, T.; Ohlson, T. Conformations of amino acids in proteins. *Acta Crystallogr.* **2002**, *D58*, 768–776.
- (43) Greenhalgh, C.; Prent, N.; Green, C.; Cisek, R.; Major, A.; Stewart, B.; Barzda, V. Influence of semicrystalline order on the second-harmonic generation efficiency in the anisotropic bands of myocytes. *Appl. Opt.* **2007**, *46*, 1852–1859.
- (44) Major, A.; Cisek, R.; Barzda, V. Femtosecond Yb:KGd(WO₄)₂ laser oscillator pumped by a high power fiber-coupled diode laser module. *Optics Express* **2006**, *14*, 12163–12168.
- (45) Orgel, J. P. R. O.; Irving, T. C.; Miller, A.; Wess, T. J. Microfibrillar structure of type I collagen *in situ*. *Proc. Natl. Acad. Sci. U.S.A.* **2006**, *103*, 9001–9005.
- (46) Bozec, L.; van der Heijden, G.; Horton, M. Collagen fibrils: nanoscale ropes. *Biophys. J.* **2007**, *92*, 70–75.
- (47) Knoesen, A. Second order optical nonlinearity in single and triple helical protein supramolecular assemblies. *Nonlinear Opt., Quantum Opt.* **2009**, *38*, 213–225.
- (48) Rocha-Mendoza, I.; Yankelevich, D. R.; Wang, M.; Reiser, K. M.; Frank, C. W.; Knoesen, A. Sum frequency vibrational spectroscopy: the molecular origins of the optical second-order nonlinearity of collagen. *Biophys. J.* **2007**, *93*, 4433–4444.